J Neurophysiol 92: 3121–3133, 2004.
First published May 5, 2004; 10.1152/jn.00234.2004.

In Vivo Mammalian Brain Imaging Using One- and Two-Photon Fluorescence Microendoscopy

Juergen C. Jung,[1,2,3] Amit D. Mehta,[1,3] Emre Aksay,[3,4] Raymond Stepnoski,[3] and Mark J. Schnitzer[1,3]

[1]*Department of Biological Sciences and Department of Applied Physics, Stanford University, Stanford, California 94305;* [2]*Department of Pharmacology, Oxford University, Oxford OX1 3QT, United Kingdom;* [3]*Bell Laboratories, Lucent Technologies, Murray Hill, New Jersey 07974; and* [4]*Department of Molecular Biology, Princeton University, Princeton, New Jersey 08544*

Submitted 8 March 2004; accepted in final form 22 April 2004

Jung, Juergen C., Amit D. Mehta, Emre Aksay, Raymond Stepnoski, and Mark J. Schnitzer. In vivo mammalian brain imaging using one- and two-photon fluorescence microendoscopy. *J Neurophysiol* 92: 3121–3133, 2004. First published May 5, 2004; 10.1152/jn.00234.2004. One of the major limitations in the current set of techniques available to neuroscientists is a dearth of methods for imaging individual cells deep within the brains of live animals. To overcome this limitation, we developed two forms of minimally invasive fluorescence microendoscopy and tested their abilities to image cells in vivo. Both one- and two-photon fluorescence microendoscopy are based on compound gradient refractive index (GRIN) lenses that are 350–1,000 μm in diameter and provide micron-scale resolution. One-photon microendoscopy allows full-frame images to be viewed by eye or with a camera, and is well suited to fast frame-rate imaging. Two-photon microendoscopy is a laser-scanning modality that provides optical sectioning deep within tissue. Using in vivo microendoscopy we acquired video-rate movies of thalamic and CA1 hippocampal red blood cell dynamics and still-frame images of CA1 neurons and dendrites in anesthetized rats and mice. Microendoscopy will help meet the growing demand for in vivo cellular imaging created by the rapid emergence of new synthetic and genetically encoded fluorophores that can be used to label specific brain areas or cell classes.

INTRODUCTION

In recent years, fluorescence imaging techniques have become increasingly useful for the study of live neurons. This stems from innovations in fluorescence microscopy (Denk and Svoboda 1997), the creation of new vital fluorophores (Miyawaki et al. 2003; Zhang et al. 2002), and the development of viral vector (Chen et al. 2000; Furuyashiki et al. 2002; Jeromin et al. 2003) and transgenic methods (Feng et al. 2000; Oliva et al. 2000) for expressing fluorescent proteins within select classes of cells. Since fluorescent probes can be used to tag specific molecular species (Lippincott-Schwartz and Patterson 2003), fluorescence imaging has been employed to monitor biochemical signaling pathways (Okubo et al. 2001; Sato et al. 2002; Zhang et al. 2002) and to map protein distributions within individual cells and across cell populations (Chiu et al. 2002; Mack et al. 2001; Oliva et al. 2000). Other imaging studies of cellular properties have relied on genetically encoded fluorescent probes that report gene expression (Brown et al. 2001; Spergel et al. 2001) or that allow determinations of cellular morphologies (Grutzendler et al. 2002; Trachtenberg et al. 2002). Neuronal dynamics may be visualized using genetically encoded fluorescent probes that indicate membrane voltage (Guerrero et al. 2002), ion concentrations (Kuner and Augustine 2000; Truong et al. 2001), or synaptic transmission (Bozza et al. 2004; Ng et al. 2002).

Unfortunately, high-resolution fluorescence imaging studies of neurons remain largely confined to in vitro preparations of cultured cells or tissue slices (Yuste et al. 2000), because of the experimental difficulties in accessing many neuron types in vivo. These difficulties chiefly concern light scattering, which leads to an exponential attenuation of light intensity with distance traveled through solid tissue. In mammalian brain, even with near infrared wavelengths of 750–900 nm that scatter less than visible light, the characteristic scattering length is only ~100 μm in mature animals (Oheim et al. 2001), 140–240 μm in young adults (Kleinfeld et al. 1998; Oheim et al. 2001), and limits fluorescence imaging depths to several hundred microns within tissue. Nonetheless, a seminal minority of fluorescence microscopy studies of individual neurons has been performed in live mammals, suggesting the possibility of forging direct links between subcellular building blocks and systems level parameters. To date, fluorescence microscopy studies of neuronal properties in live mammals have been limited to superficial or easily accessible tissues, such as trigeminal nerve terminals (Harris and Purves 1989), parasympathetic ganglia (Harris and Purves 1989; Pomeroy and Purves 1988; Purves and Lichtman 1987; Purves et al. 1987), and neuromuscular junctions (Akaaboune et al. 2002; Balice-Gordon and Lichtman 1994; Walsh and Lichtman 2003), or to within ~500 μm of the neocortical (Grutzendler et al. 2002; Helmchen et al. 1999; Stosiek et al. 2003; Svoboda et al. 1997, 1999; Trachtenberg et al. 2002) or olfactory bulb (Charpak et al. 2001) surface. Recently, use of a Ti:sapphire regenerative amplifier as an excitation source for ultra-deep two-photon microscopy has been explored (Beaurepaire et al. 2001; Theer et al. 2003). This source has enabled a demonstration in which fluorescent neuronal cell bodies were visualized up to 850–1,000 μm deep within the neocortex of 3-wk-old mice (Theer et al. 2003). However, most mammalian brain regions, which are not superficial and lie deeper than 500–1,000 μm within tissue, have remained inaccessible to cellular-level fluorescence imaging in vivo.

Our goal was to develop high-resolution fluorescence imaging within deep brain areas that have been unreachable by optical microscopy, because this would open entirely

Address for reprint requests and other correspondence: M. J. Schnitzer, Stanford Univ., James H. Clark Center, Stanford CA 94305-5435 (E-mail: mschnitz@stanford.edu).

The costs of publication of this article were defrayed in part by the payment of page charges. The article must therefore be hereby marked "*advertisement*" in accordance with 18 U.S.C. Section 1734 solely to indicate this fact.

new possibilities for studying cellular biology in vivo. We constructed fluorescence microendoscopes that exhibit a smaller range of diameters (350–1,000 μm) and higher resolution (as good as 0.86 μm) than previous miniature fluorescence endoscopes, which exhibit 1–8 mm diam and 1.8–3.1 μm resolution at best (Knittel et al. 2001; Rouse and Gmitro 2000; Sabharwal et al. 1999). Toward this end, we introduced microendoscope probes comprised of multiple gradient refractive index (GRIN) micro-lenses that are 350–1,000 μm in diameter and that provide micron-scale resolution (Jung and Schnitzer 2003). These probes enable minimally invasive in vivo imaging of individual cells in deep tissues (Jung et al. 2003; Levene et al. 2003, 2004). Unlike conventional lenses that refract light at curved surfaces, GRIN lenses are not ground to shape and so are cheaply fabricated in sub-millimeter sizes (e.g., 100–1,000 μm) suitable for insertion into solid tissue (Emkey and Jack 1987; Messerschmidt et al. 1997; Reed et al. 2002). In microscopy, it is well known that one- and two-photon fluorescence imaging modalities have complementary strengths and weaknesses, and we sought to develop both modalities in the microendoscopy format. Although use of only a single GRIN lens for microendoscopy suffers from several optical drawbacks (Levene et al. 2002, 2004), early work exploring use of compound doublet GRIN micro-lenses for in vivo one-photon microendoscopy (Jung and Schnitzer 2002; Jung et al. 2002) and use of doublet (Jung et al. 2002, 2003) and triplet GRIN micro-lenses (Jung and Schnitzer 2003; Jung et al. 2003; Levene et al. 2003, 2004) for in vitro and in vivo two-photon microendoscopy appears promising.

Here we describe in vivo one- and two-photon fluorescence microendoscopy. The strengths and weaknesses of these two modalities resemble those of one- and two-photon fluorescence microscopy, respectively. One-photon fluorescence imaging offers the advantages of full-frame image acquisition, lower cost, and greater ease of use. Although one-photon microendoscopy lacks optical sectioning capabilities, as with one-photon microscopy lack of sectioning can also be used to advantage, because it allows signals originating from different depths to be aggregated toward achieving faster frame-rates. Two-photon imaging involves laser-scanning and provides localized fluorescence excitation that yields inherent optical sectioning and minimal phototoxicity outside the focal waist (Hopt and Neher 2001). Because essentially all fluorescence photons originate from the focal spot, even photons that scatter in tissue en route to the photodetector can contribute to image signals (Denk and Svoboda 1997). Thus two-photon imaging is especially well suited for imaging through hundreds of microns of biological tissue.

Using one-photon microendoscopy we obtained video-rate movies of individual red blood cells moving within neocortical, hippocampal, and thalamic capillaries of anesthetized rats and mice. We also visualized multiple hippocampal pyramidal cells within single image frames acquired in the CA1 area of anesthetized mice. Using two-photon microendoscopy in anesthetized rats and mice, we imaged individual neurons and dendrites in the CA1 hippocampal area, up to ~270 μm away in tissue from the face of the endoscope.

METHODS

Microendoscope probes based on gradient refractive index micro-lenses

GRIN lenses exhibit a spatially varying refractive index, because the glass is inhomogeneously doped with a cation species, such that cation density is typically highest at the central axis of the lens and declines toward the periphery (Gomez-Reino et al. 2002; Messerschmidt et al. 1997). This leads to a refractive index profile that declines approximately quadratically with radial distance from the central axis of the lens (Gomez-Reino et al. 2002; Reed et al. 2002). In a ray description, total internal reflection occurs in a gradual manner as light passes from central regions to peripheral regions of lower index, causing light rays to travel down the cylindrical lens axis in an approximately sinusoidal path (Gomez-Reino et al. 2002). The axial length for one full sinusoidal cycle is called the pitch length, P, of the GRIN medium and is determined by the refractive index profile. Two lenses made from the same GRIN substrate but of different pitch (e.g., ½-pitch versus ¼-pitch) will have distinct lensing properties (Emkey and Jack 1987). Decreasing P leads to an increased numerical aperture (*NA*). Using combinations of GRIN micro-lenses with different *NA*, we have developed endoscope probes for both one- and two-photon fluorescence imaging.

Endoscope probes were custom fabricated thallium-doped GRIN relay lenses (NSG) and thallium-doped (NSG) and silver-doped objectives (GrinTech) glued together with optical epoxy (Fig. 1*A*). Such lenses use cylindrical GRIN substrate with an index of refraction, n, that varies approximately quadratically with radius, r: $n(r) = n_0(1 - g^2r^2/2)$, where n_0 is the refractive index on the lens axis. A substrate's pitch length, P, is determined by the quadratic coefficient g, $P = 2\pi/g$.

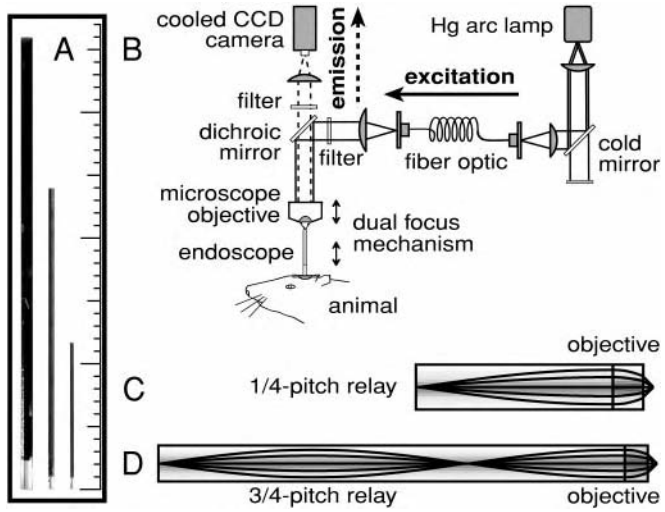

FIG. 1. Optical designs for one-photon fluorescence endoscopy. *A*: photograph of three gradient refractive index (GRIN) doublet microendoscope probes, 1,000-, 500-, and 350-μm diam, oriented with objective lens down. The relay lenses exhibit a dark coating. One minor tick on the scale equals 1.0 mm. *B*: optical layout used for the endoscopic studies of Figs. 2–5. A mercury (Hg) arc lamp provides fluorescence excitation light, which reflects off a cold mirror and couples into a 1-mm diam optical fiber. Excitation light passes through a fluorescence excitation filter and is deflected onto the main optical axis by a dichroic mirror. A microscope objective lens delivers the excitation light into the microendoscope probe. The imaging plane in the sample may be adjusted by moving either the probe or the microscope objective. Fluorescence emissions (dashed lines) pass back through the microendoscope probe, microscope objective, dichroic mirror, and an emission filter, and are focused onto a CCD camera. *C*: optical diagram of light rays in a doublet microendoscope probe with a relay lens of length ¼-pitch. An object that is located at the working distance of the endoscopic objective lens is imaged just outside the external face of the relay lens. *D*: optical diagram of light rays in a doublet microendoscope probe with a ¾-pitch relay.

The endoscope probes used for one-photon imaging are micro-lens doublets, 350–1,000 μm in diameter (Fig. 1*A*), comprised of an endoscope objective lens and a much longer but weaker relay lens. The objective lens is less than ¼-pitch in length, and in our current probes has a relatively high *NA* of near 0.5 for micron-scale imaging. Our endoscope objectives have an infinity design, in that they collimate light from a point source residing at the working distance of the endoscope probe. The relay lens is made from a GRIN substrate with a longer pitch length, so this lens has a lower *NA* (0.084–0.11). The relay focuses a real image of the specimen slightly outside the back face of the endoscope probe (Fig. 1, *C* and *D*) with a magnification typically between 4–6×. A primary function of the relay is to provide sufficient length for insertion into deep tissue. In monochromatic light, the higher *NA* objective lens, not the lower *NA* relay, limits the optical resolution. There are several options for relays of different length. The shortest relay is ¼-pitch (Fig. 1*C*) and the next shortest is ¾-pitch (Fig. 1*D*). If needed, additional length can be added to the relay in integral multiples of ½-pitch. Optical aberrations accrue in GRIN lenses of longer pitch (Gomez-Reino et al. 2002), so it is advisable to choose a relay lens that is as short as possible, but long enough to reach the tissue under study.

To relate the *NA*, working distance (*WD*), focal distance (f), field of view (*FOV*), and lateral magnification (M_L) of our endoscope probes to the properties of the GRIN substrates, we used the matrix formulation of paraxial ray optics (Kogelnik 1965). Although more detailed design can be performed using numerical ray tracing, this analytical treatment provides insight and satisfactory agreement with experimental values for many purposes. A GRIN objective lens that is immersed in a sample medium of refractive index n_m and that possesses a diameter d, length L, and radial refractive index profile $n_{ob}(r) = n_{ob,0}(1 - g_{ob}^2\, r^2/2)$ will focus collimated rays entering one face of the objective to a focal spot a working distance

$$WD = \frac{n_m \cot(g_{ob}L)}{n_{ob,0}\, g_{ob}}$$

from the opposite face (Fig. 1, *C* and *D*). This focal spot lies a focal distance

$$f = \frac{n_m \csc(g_{ob}L)}{n_{ob,0}\, g_{ob}}$$

from the principal plane. The *NA* of the objective lens is

$$NA = n_m \sin\left(\tan^{-1}\left(\frac{d n_{ob,0}\, g_{ob} \sin(g_{ob}L)}{2n_m}\right)\right) = n_m \sin\left(\tan^{-1}\left(\frac{d}{2f}\right)\right)$$

which is $\frac{n_m d}{2f}$ in the paraxial approximation. For the doublet designs of Fig. 1, in which a GRIN objective lens of $0 < L < ¼P$ is combined with a relay lens that is ¼*P* modulo ½*P* (i.e., ¼*P*, ¾*P*, etc.; Fig. 1, *C* and *D*) and that possesses a refractive index profile $n_R(r) = n_{R,0}(1 - g_R^2\, r^2/2)$, a real image of the specimen is focused at the external face of the relay lens with lateral magnification

$$|M_L| = \frac{n_{ob,0}\, g_{ob} \sin(g_{ob}L)}{n_{R,0}\, g_R}$$

and field of view

$$FOV = \frac{d n_{R,0}\, g_R}{n_{ob,0}\, g_{ob}} \csc(g_{ob}L)$$

We have used *WD* values between 130–1,040 μm. Since the refractive indices of various brain tissues are uncertain, all calculated values of *WD* reported in this paper are for a water medium ($n_m = 1.3$). The number of internal image planes within the probe determines the sign of the magnification, with an image inversion occurring at each image plane.

With two-photon imaging, we sometimes used a triplet design comprised of an endoscopic objective lens, a ½-pitch relay lens, and a ¼-pitch coupling lens made of the same GRIN substrate as the objective (Fig. 6*C*). In this case, the relay lens acts as a telescope of magnification minus one. Although the use of the ½-pitch relay and the addition of the coupling lens do not change the above formulae for *WD* and *FOV*, the expression for M_L simplifies: $M_L = \sin(g_{ob}L)$.

The microendoscope probes were held within the optical instrumentation using custom-made aluminum holders shaped like an hourglass with a hole along the axis. Probes were afforded some flexibility to pivot about the hourglass waist by encasing the probes in silicon tubing before placing them into the holder.

One-photon microendoscopy

The one-photon fluorescence endoscope was constructed on a rail (X95, Newport, Irvine, CA) and was mounted on a translation stage (XYR-8080, New England Affiliated Technologies, Lawrence, MA) driven by a stepper motor controller (MP285, Sutter, Novato, CA). Key optical components include a binocular (452934, Zeiss) and eyepieces (444034, Zeiss). Light from a mercury arc lamp (HBO 100, Zeiss) is coupled into a 1.0-mm-diam fiber (Multimode Fiber Optics, East Hanover, NJ) as part of an illumination scrambler (Inoue and Spring 1986). After passing through a wheel (Linos) of fluorescence excitation filters (Chroma, Rockingham, VT), the excitation light is collected by a Leitz H 32× 0.6 *NA* objective and a Hastings triplet lens (Edmund Optics, Barrington, NJ) and deflected onto the main optical axis by one of several exchangeable dichroic mirrors (Chroma) such that the light overfills the back aperture of a microscope objective. The objective delivers the light to the endoscope probe (Fig. 1*B*).

Fluorescence emissions return back through the endoscope probe, microscope objective, dichroic mirror, and a wheel (Linos) of emission filters (Chroma). Images can be viewed through the eyepieces of the binocular or projected onto a camera. For imaging neurons stained with Di-I, we used the fluorescence filter set HQ535/50-Q565LP-HQ610/75 (Chroma) and a cooled CCD camera (Coolsnap HQ, Roper) controlled by commercial imaging software (V^{++}, Digital Optics; IPLab, Scanalytics, Fairfax, VA). Red blood cell imaging involved the filter set HQ470/40-Q495LP-HQ525/50 or -HB535/30 (Chroma) and a monochrome CCD camera (XC-ST70, Sony). Movies were stored on DV tape using a digital video recorder (DCR-TRV900, Sony). Imaging in YFP-H mice involved a HQ470/40-Q495LP-HQ535/30 filter set and the cooled CCD camera.

There are two mechanisms for focusing the image, implemented through a pair of modular focus units (81705, Nikon) that hold the microscope objective and endoscope probe. One unit adjusts the position of the endoscope probe within the animal. The second unit adjusts the position of the microscope objective relative to the endoscope probe; therefore the image focus within tissue can be altered without any mechanical movements within the animal.

Optical resolution measurements

Spatial calibration of the endoscope's motorized *X-Y* stage was performed using a stage micrometer with a 10-μm grid imaged under transmitted light provided by a light box (455136, Zeiss). To estimate the fluorescence intensity point spread function, we prepared microscope slides with individual 170-nm-diam fluorescence beads (P7220, Molecular Probes, Eugene, OR) fixed to the slide surface. A clean slide was washed in 1 M NaCl and a coverslip (no. 1.5, Corning, Corning, NY) was fixed on the slide using double-sided tape as an adhesive spacer. We filled the chamber with a solution of fluorescence beads and waited about 1 min for beads to adhere to the coverslip. We then flushed the chamber with water to remove any beads remaining in solution and allowed the chamber to dry in air.

Fluorescence beads were epi-illuminated under the one-photon endoscope, and images were filtered using a band-pass (HQ535/30)

and acquired at 12-bit resolution with the cooled CCD camera. The images were imported into image analysis software (NIH Image) and one-dimensional cross sections through the bead center were normalized in amplitude and then fit with an Airy disk, $f(x) = [2J_1(kx)/(kx)]^2$ (Diaspro 2002). The full width at half-maximum (FWHM) of the Airy disk was obtained from its inverse proportionality to the fitting parameter, k. Standard errors were obtained using the distribution of FWHM values measured over a population of beads.

Tests of optical resolution using grid lines were performed using a Ronchi ruling (600 lines/mm, Edmund Optics) or a Marine Biological Laboratory/National Nanofabrication Facility (MBL/NNF) transmittance test slide (Oldenbourg et al. 1993). The MBL/NNF slide exhibited a Siemens star and grid lines at a variety of spacings. Resolution was estimated using the Siemens star by determining the radius at which image contrast between adjacent wedges disappears. Errors in radial measurements yielded errors in resolution values.

Two-photon microendoscopy

The two-photon endoscope was constructed on an X95 rail (Newport) mounted on a stepper motor driven *X-Y* translation stage (New England Affiliated Technologies). This instrument was built as a modification to a previously existing two-photon microscope (Svoboda et al. 1997). A wavelength-tunable ultra-short pulsed Ti:sapphire laser (Tsunami, Spectra-Physics, Mountain View, CA) pumped by a 10 W Nd:YVO_4 laser (Millenia, Spectra-Physics) provides ~100-fs pulses of near infrared light for fluorescence excitation. A pair of galvanometer-driven deflector mirrors (Cambridge Technologies, Cambridge, MA) steer the excitation beam in two angular dimensions as controlled by custom written imaging software (Confoc, Raymond Stepnoski). The beam passes through a scan lens (4524268033, Zeiss), a dichroic mirror, and a binocular tube lens (Zeiss), and overfills the back aperture of a microscope objective lens that focuses the beam just above the top face of either a doublet or triplet GRIN endoscope probe. Scanning the laser focal spot in this plane leads to scanning of the focal spot in the specimen image plane.

Anesthetized animals were placed underneath the endoscope probe. The focal plane of the excitation beam within the brain can be adjusted using a custom-built dual-focus mount based on two translation stages (Newport) and two stepper motors. A photomultiplier tube (R3896, Hamamatsu) was used to detect fluorescence returning through the endoscope probe (Figs. 6 and 7). A computer controls the scanning of the galvanometer mirrors and constructs the digital image. In vitro tests of lateral optical resolution had shown that with probes of near 0.5 *NA* two-photon microendoscopy attains 1–2 μm resolution (Jung and Schnitzer 2003). For imaging Di-I–labeled neurons, the laser wavelength was tuned to 815 nm, and for imaging YFP mice, the laser was tuned to 910–925 nm. Typical laser excitation power at the sample was 25–50 mW.

Animals and surgery

All animal procedures were performed in accordance with National Institutes of Health guidelines and were approved by the Bell Laboratories and Stanford University Institutional Animal Care and Use Committees.

Adult female Sprague-Dawley rats were anesthetized with urethane (1.5 mg/g body weight, ip) or ketamine and xylazine (0.13 and 0.01 mg/g body weight, ip, respectively). Body temperature was monitored with a rectal probe and was kept stable at 36°C with a feedback-controlled heat blanket (Harvard Apparatus, Holliston, MA). The head was shaved, and the eyes were covered with ointment (Puralube Vet, Pharmaderm, Melville, NY). An incision was made through the scalp along the midline for a length of 1–1.5 cm. The skin was retracted, and the skull was exposed. A craniotomy was performed over the brain area of study.

We used two general methods for reaching deep brain tissue with the microendoscope probe. The first method involved gradually lowering the probe through brain matter until it reached the area of interest. Thus for our initial studies in rat somatosensory cortex, a 2-mm diam craniotomy was performed at stereotaxic coordinates 4 mm lateral, −3 mm from bregma. After dye labeling (see next section), the endoscope probe was gradually lowered 1 mm ventral into tissue perpendicular to the cortical surface. The brain surface was washed with artificial cerebral spinal fluid (ACSF) and imaging commenced. ACSF was composed of (in mM) 125 NaCl, 5 KCl (Baker), 10 glucose, 10 HEPES, 2 ($MgSO_4 \cdot 7\ H_2O$) (Fisher Scientific), and 2 ($CaCl_2 \cdot 2\ H_2O$) (all chemicals are from Sigma except where noted). Although this method for inserting the microendoscope into tissue is similar to that used previously (Levene et al. 2004) and yielded crisp images of both neurons and blood cell dynamics, we were concerned about the possibility of compression of brain tissue that might depress neuronal activity (Bolay et al. 2002). Thus, during studies of the CA1 hippocampal area and of lateral dorsal thalamus, we employed a second method that is an intermediate between our first approach and a surgical method recently developed for imaging hippocampus in vivo by conventional microscopy (Mizrahi et al. 2004).

After aspirating overlying neocortex in the anesthetized mouse, it is possible to use a conventional microscope objective to image fluorescent hippocampal pyramidal cells (Mizrahi et al. 2004). Although this approach does obviate concerns about compression of overlying tissue, aspiration of large portions of neocortical matter is highly invasive. We developed an intermediate approach in both rats and mice in which prior to insertion of the endoscope probe, we removed a thin column of tissue overlying the brain area of interest. We then inserted the endoscope through this opening. The brain area under observation was left intact. With experience, we were able to image through smaller craniotomies (about 1.5 mm) and with correspondingly less tissue removed, without noticeable effects on image quality. This method allowed us to image the rat laterodorsal thalamus in vivo, slightly less than 4 mm below the neocortical surface, which is prohibitive with conventional microscopy even after large-scale surgical removal of neocortical matter.

For studies of rat hippocampus, a 1.5- or 3.0-mm-diam craniotomy centered at coordinates 1.9 mm lateral, −4.0 mm from bregma was opened. The dura was removed with forceps. Bent and blunted needles (23 and 26 gauge) were used to aspirate a column of tissue from overlying neocortex and corpus callosum that had a diameter slightly smaller than that of the craniotomy. The dorsal alveus layer of hippocampus remained untouched and intact. During aspiration, fine control of suction strength was performed by partially covering a 1-mm hole drilled in the plastic fitting of the suction needle. The corpus callosum and any clotted blood was removed by washing with ACSF while aspiration suction was reduced.

Endoscopic imaging studies of rat laterodorsal (LD) thalamus were performed using a 2.0-mm-diam craniotomy centered at 2.4 mm lateral, −3.5 mm bregma or at 1.9 mm lateral, −3.0 mm bregma. Overlying neocortical and hippocampal tissue within the diameter of the craniotomy were aspirated. LD was untouched and left intact.

Female mice were anesthetized with injection of ketamine (0.13 mg/g ip) and xylazine (0.01 mg/g ip). The head was shaved and eyes were covered with eye ointment. For imaging in CA1 a 1.5- or 2.0-mm-diam craniotomy at coordinates 2.0 mm lateral, −2.0 mm from bregma was opened. Neocortex and corpus callosum were aspirated over a diameter the same as that of the craniotomy. The alveus layer of hippocampus was untouched and remained intact.

Fluorescence labeling

For red blood cell imaging, fluorescein (0.8 mg/kg body weight dissolved in ACSF, Sigma-Aldrich, St. Louis, MO) was injected into

the femoral vein of rats and mice with a 30-gauge needle. The injection was done under a surgical stereoscope to ensure that dye was only injected into the circulation and not into adjacent tissue.

Rat neocortical neurons were labeled using Di-I paste (Molecular Probes). The tip of a glass microelectrode of ~3 MΩ impedance was dipped into the paste and inserted up to 1 mm into the cortex. The microelectrode was then removed. After waiting ~30 min or longer for the dye to diffuse, individual neurons at the periphery of the microelectrode's path through tissue were visible. The endoscope was then inserted into tissue adjacent to the insertion point of the microelectrode.

Imaging studies of fluorescent CA1 hippocampal neurons in live mice involved the YFP-H transgenic line that expresses yellow fluorescent protein (YFP) under control of neuron-specific elements from the *thy1* gene (Feng et al. 2000).

RESULTS

One-photon fluorescence microendoscopy

Despite important differences regarding instrument size and lens design, the instrument that we built for one-photon fluorescence microendoscopy exhibits many of the strengths and weaknesses of conventional epi-fluorescence microscopes (Fig. 1). Epi-fluorescence imaging typically employs incoherent illumination, which we provided using a Mercury-arc lamp, and enables direct viewing through eyepieces or image capture on a pixilated detector such as a CCD or photodiode array (Yuste et al. 2000) (Fig. 1*B*). Our instrument uses conventional epi-fluorescence filter sets and a microscope objective that couples fluorescence excitation light into a compound doublet microlens probe (350–1,000 μm diam; Fig. 1*A*) comprised of a GRIN endoscopic objective lens and a GRIN relay lens (Fig. 1, *C* and *D*). This microendoscope probe delivers the illumination to the tissue and projects a real epi-fluorescence image to the external face of the relay lens (METHODS; Fig. 1, *C* and *D*), at the front focal plane of the microscope objective (Fig. 1*B*). A benefit of our design is that there are two mechanisms for focusing the image. One mechanism adjusts the position of the endoscope probe within the animal. After the initial position of the endoscope probe is set in tissue, it is often advantageous to keep the probe stationary. The second mechanism adjusts the position of the microscope objective relative to the probe, so that the image focus can be altered without any mechanical movements within the animal.

To estimate endoscope resolution, we performed three different tests. First, we imaged grids that were nanofabricated by electron lithography (Oldenbourg et al. 1993). With three endoscopes of *NA* from 0.38–0.47, we found that grids with 1.66- or 1.2-μm spacing could be sharply resolved (Fig. 2*A*). These same three endoscopes barely resolved a grid of 1.0-μm spacing, and the images of this grid exhibited poor contrast (Fig. 2*A*, *bottom inset*). This indicates that the optical resolution of these endoscopes according to the Sparrow criterion of zero contrast (Diaspro 2002) is only slightly better than a micron.

Second, we imaged a test plate exhibiting a nanofabricated Siemens star (Oldenbourg et al. 1993), which is a circular pattern containing 36 pairs of alternating transparent and opaque wedges (Fig. 2*B*, *inset*). The radius from the center of the star at which the image contrast between adjacent wedges disappears provides a measure of resolution according to the Sparrow criterion (Diaspro 2002; Oldenbourg et al. 1996). This method provided resolution estimates of 0.86 ± 0.07, 0.88 ± 0.08, and 0.92 ± 0.15 μm for the endoscopes of 0.47, 0.46, and 0.38 *NA*, respectively.

Third, we imaged subresolution 170-nm fluorescent beads (Fig. 2*B*), which mimic a point source of fluorescence and allow one to study the intensity point spread function of an optical instrument (Diaspro 2002). We determined FWHM values of 0.89 ± 0.01, 0.98 ± 0.02, and 1.16 ± 0.1 μm for the endoscopes of 0.47, 0.46, and 0.38 *NA*, respectively. The FWHM is ~7% broader than the minimum separation at which two identical Airy disks sum so that their distinct peaks can just

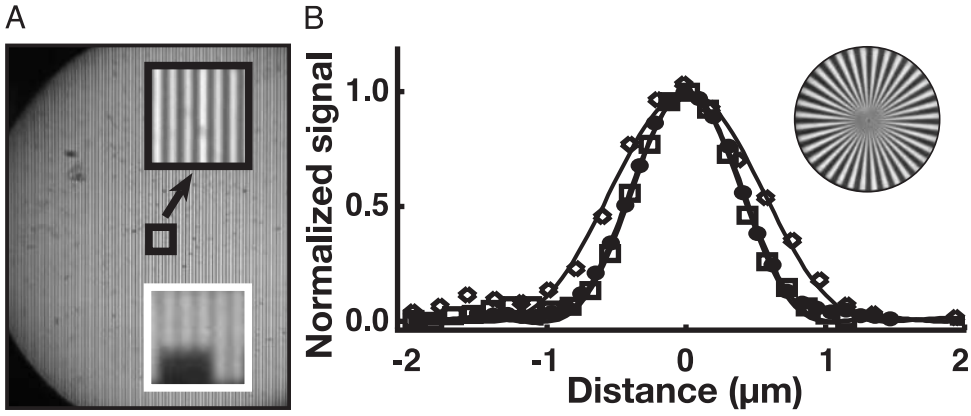

FIG. 2. Three methods for determination of endoscope resolution. *A*: image of a ruled grid of 1.6-μm-spacing obtained with a 1,000-μm diam endoscope possessing a 390-μm working distance (*WD*) and 0.46 *NA*. The image extends to the circular perimeter of the endoscopic relay, visible in the left of the photo. *Top inset*: magnified image of six grid lines, taken from the area boxed in black. *Bottom inset*: magnified image of six grid lines obtained using the same microendoscope probe and a grid of 1.0-μm spacing. *B*: one-dimensional image profiles of single 170-nm fluorescent beads, acquired in an axial plane through the bead center. Intensity values are normalized to maximum intensity at the bead center. □, data for a 500-μm-diam endoscope with 0.47 *NA* and 130-μm *WD*; ●, data for a 1,000-μm-diam endoscope with 0.46 *NA* and 390-μm *WD*; ◇, data for a 1,000-μm-diam endoscope with 0.38 *NA* and 1040-μm *WD*. There are three solid lines, which are parametric fits to an Airy disk, $f(x) = [2J_1(kx)/(kx)]^2$, but two of these lines are nearly indistinguishable. *Inset*: image of a Siemens star, taken with the same 500-μm-diam endoscope used to image fluorescent beads.

barely be distinguished, as in the Sparrow criterion (Diaspro 2002). Thus these values are consistent with those obtained using the Siemens star.

Video-rate microendoscopy of red blood cell dynamics in deep brain areas

Our first in vivo experiments with one-photon microendoscopy in the mammalian brain involved visualization of cerebral blood flow and red blood cell dynamics. Cerebral blood flow and metabolism constitute important biomedical topics, not only because of the clinical relevance to stroke and ischemia (Dijkhuizen et al. 2001) and migraine (Bolay et al. 2002), but also because further study of the coupling between neural activity and vascular response is needed toward understanding the physiological underpinnings of brain imaging modalities that rely on vascular and metabolic effects (Fox et al. 1986; Martin et al. 2002; Ogawa et al. 1992; Shtoyerman et al. 2000). Prior imaging studies have examined mammalian blood flow in the pia (Hudetz et al. 1997; Ma et al. 1974) and in the upper 250 μm (Dirnagl et al. 1992; Villringer et al. 1994) or upper 600 μm (Kleinfeld et al. 1998) of neocortex. As we describe below, in vivo video-rate microendoscopy can now be used to visualize blood flow in individual vessels deep within the live rodent brain.

We examined blood cell dynamics by injecting the fluorescent dye fluorescein into the blood stream. This provides a background label of blood plasma, causing the red blood cells, which are ~8 μm in diameter, to appear dark by comparison (Kleinfeld et al. 1998). Video-rate movies of blood flow revealed trajectories of individual red blood cells in larger vessels and capillaries in rat neocortex (data not shown), mouse hippocampus (Fig. 3*A*, Movie 1), rat hippocampus (Fig. 3*B*, Movie 2), and rat thalamus (Fig. 3*C*, Movie 3). Blood cell speeds in capillaries varied widely, generally over the range of ~30–350 μm/s, which is within the broad range of speeds observed in prior imaging studies of capillary blood flow in the pia and neocortex (Dirnagl et al. 1992; Hudetz et al. 1997; Ivanov et al. 1985; Kleinfeld et al. 1998; Ma et al. 1974; Villringer et al. 1994). In capillaries, individual red blood cells were particularly apparent and often progressed forward in an irregular manner, occasionally even reversing direction momentarily. Such irregular red blood cell motion has been observed previously in neocortex (Kleinfeld et al. 1998). Because video-rate movies convey a much stronger sense of individual blood cell motions than do still frames, readers are

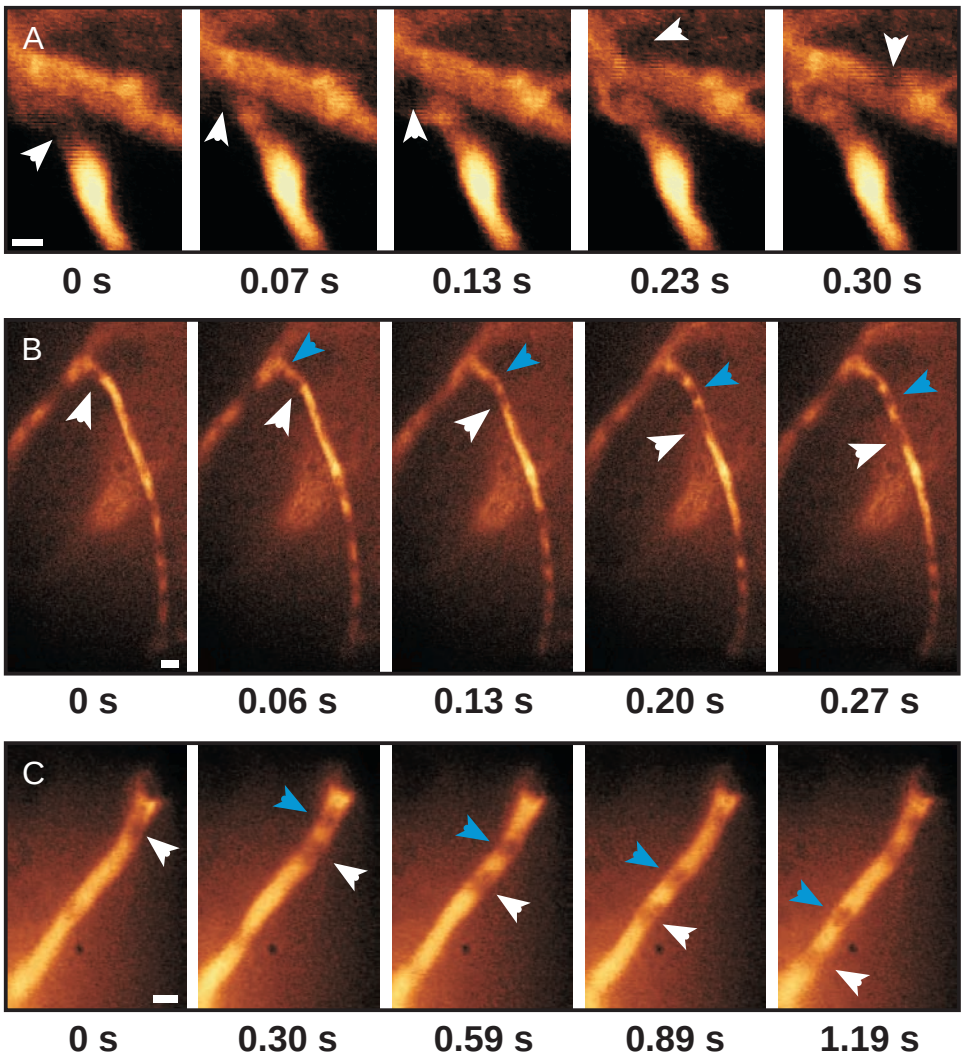

FIG. 3. Movie frames of single red blood cell dynamics visualized in vivo using one-photon fluorescence microendoscopy. Compressed versions of these movies may be viewed in Data Supplements. Relative times in seconds are below each movie frame. Blue and white arrowheads point to individual red blood cells and track the cells' progress within the vessels. *A*: sequence of movie frame images from the CA1 hippocampal area of a live mouse. This is an example of a "to-and-fro" flow pattern. *B*: sequence of movie frame images from CA1 hippocampus of a live rat. *C*: sequence of movie frame images from the laterodorsal thalamic nucleus of a live rat. All fluorescence images are presented in a pseudocolor scale, but no enhancement or filtering of raw image data has been performed. Frames in *A–C* were obtained with a 1,000-μm endoscope of 390-μm *WD* and 0.46 *NA*. Scale bars are 10 μm.

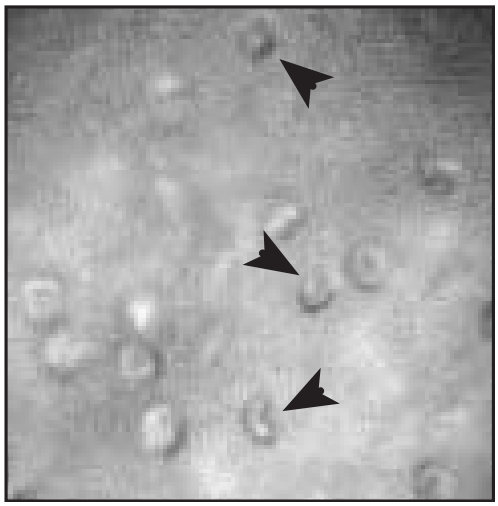

FIG. 4. Still frame of individual red blood cells in rat somatosensory cortex, taken with the same microendoscope used for Fig. 3. Biconcave red blood cell structures are readily apparent (black arrowheads).

encouraged to view movie data (available in compressed form in Supplementary Information, Movies 1–3)[1] that formed the basis for the still-frame sequences shown in Fig. 3. Endoscopic images of individual red blood cells exhibited the biconcave structure of these cells (Fig. 4), showing our capacity to resolve subcellular micron-scale details in vivo. Because of the lack of optical sectioning in one-photon fluorescence endoscopy, fluorescent blood vessels that were out of the image focal plane were often apparent. This did not prove to be a major obstacle to achieving video-rate imaging of blood cell dynamics in brain areas that have been inaccessible to conventional microscopy.

In vivo neuronal imaging using one-photon microendoscopy

To demonstrate our ability to visualize neurons deep within live mammals, we examined neocortical neurons in anesthetized rats and hippocampal neurons in anesthetized mice. To label rat neurons in somatosensory cortex, we used the lipophilic fluorescent dye, Di-I, which binds to and diffuses along lipid membranes (METHODS). After delivery of dye into infragranular layers of somatosensory cortex, allowance of sufficient time for the dye to label neuronal processes, and insertion of the microendoscope probe into neocortex 1 mm ventral to the pia, we were able to visualize individual fluorescent cells and dendrites (e.g., Fig. 5*A*).

To demonstrate endoscopic imaging in mice, we used transgenic mice in which a subset of hippocampal pyramidal cells express the yellow fluorescent protein (YFP) (Feng et al. 2000). With the endoscope probe positioned dorsally above the hippocampal alveus, fluorescent dendrites in stratum oriens were visible (Fig. 5*B*). By adjusting the focus of the microscope objective external to the animal but without adjusting the position of the endoscope probe, we also visualized small clusters of individual pyramidal cell bodies lying more ventrally in stratum pyramidale (Fig. 5, *C* and *D*), about 180–220 μm below alveus.

These data show that one-photon microendoscopy can be used to visualize individual neurons in vivo. As demonstrated in the YFP-H animals, the method provides a convenient means of detecting fluorescent proteins within both dendritic and somatic cellular compartments in deep brain neurons in vivo, which should be applicable to the study of other transgenic animal lines. As with conventional epi-fluorescence microscopy, when imaging a specimen embedded deep within tissue, there is a fluorescence background from out of focus and scattered fluorescence emissions (Fig. 5, *C* and *D*). Thus, to provide three-dimensional sectioning and to increase image contrast, we developed in vivo laser-scanning two-photon microendoscopy.

Laser-scanning two-photon fluorescence microendoscopy

In our previous work, we developed two-photon microendoscopy using a GRIN triplet endoscope probe (Jung and Schnitzer 2003). In this study, we explored several variants of our original strategy for laser scanning (Fig. 6). One variant uses a doublet endoscope probe comprised of an endoscope objective lens and a ¼-pitch relay lens (Fig. 6*A*), nearly identical to the probe depicted in Fig. 1*C* for one-photon imaging. (Minor differences concern the distinct wavelengths used.) A low *NA* achromatic coupling lens focuses the laser beam just above the face of the endoscope relay lens (Fig. 6*A*), and a pair of galvanometer-driven deflector mirrors scans the focal spot laterally in two dimensions (Fig. 7). The endoscope probe translates the demagnified focal spot and its scan pattern onto the sample focal plane (Fig. 6*A*). A portion of the fluorescence emissions returns through the endoscope probe, is

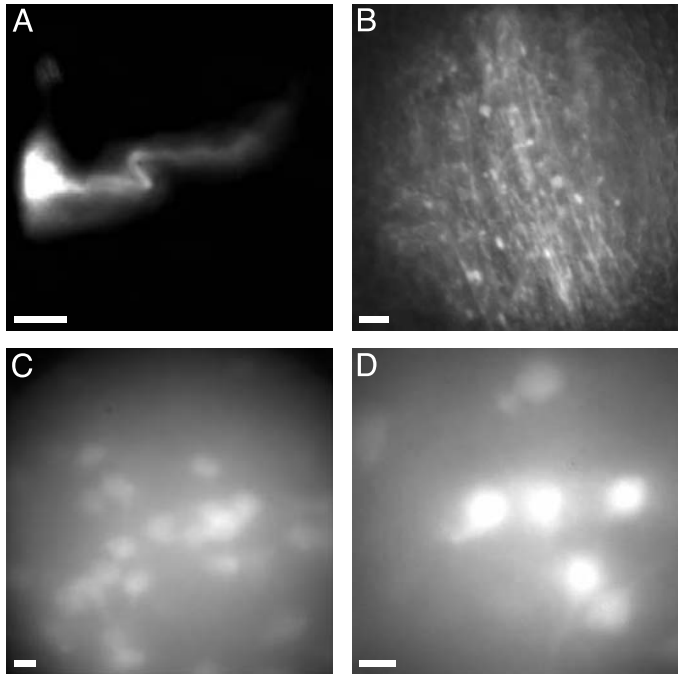

FIG. 5. Mammalian neurons imaged in vivo using one-photon fluorescence microendoscopy. *A*: fluorescent Di-I-labeled neuron imaged within infragranular somatosensory cortex in an anesthetized rat, visualized with a 1,000-μm-diam endoscope probe with 130-μm *WD* and 0.48 *NA*. *B–D*: CA1 hippocampal pyramidal cells in anesthetized YFP-H mice were visualized with a 1,000-μm-diam endoscope probe with 390-μm *WD* and 0.46 *NA* positioned above the alveus. Without moving the probe, the image was focused *B*, on basal dendrites in stratum oriens, or *C* and *D*, on pyramidal cell bodies in stratum pyramidale. Scale bars are 10 μm.

[1] The Supplementary Material for this article (three movies) is available online at http://jn.physiology.org/cgi/content/full/00234.2004/DC1.

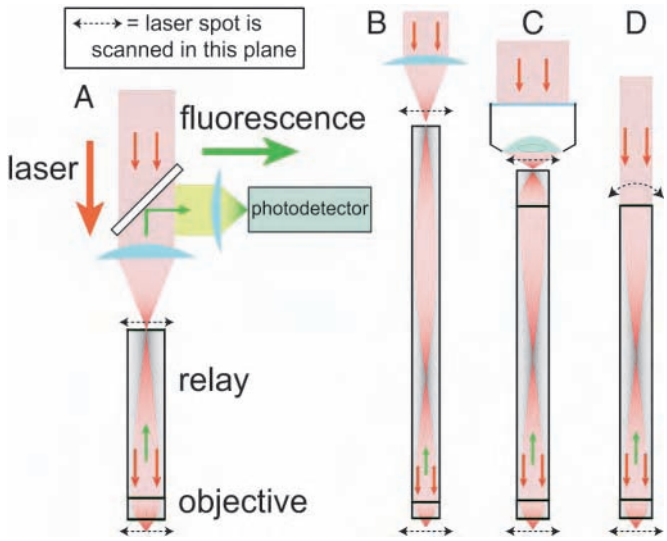

FIG. 6. Laser-scanning strategies for two-photon fluorescence endoscopy. *A*: a simple scanning strategy involves a microendoscope probe with a ¼-pitch relay lens (Fig. 1*C*). The collimated laser beam (red arrows) is focused onto the back face of the endoscope probe with an achromatic lens that provides a low *NA* focus matching that of the endoscopic relay lens. To achieve this low *NA* focus, the laser beam may underfill the lens aperture of the coupling lens, as shown. The laser focus is scanned across the face of the endoscopic relay lens (dashed arrow line). The probe demagnifies and translates the scanning pattern to the image plane within the tissue sample (dashed arrow line). A portion of the two-photon excited fluorescence (green arrows) that is induced at the sample focal spot returns through the endoscope probe and is separated from the laser excitation by a dichroic mirror. A lens focuses the fluorescence onto a photodetector. There are several variants of this strategy; for simplicity, the dichroic mirror and detection optics are omitted from *B–D*. *B*: this scanning strategy is identical to that shown in *A* except that an endoscope probe with a ¾-pitch is used (Fig. 1*D*). *C*: a scanning strategy using a triplet endoscope probe. The probe is comprised of an objective lens, a relay lens, and a ¼-pitch GRIN coupling lens with 0.5 *NA*, matching the *NA* of a 0.5 *NA* microscope objective that couples the excitation laser light into the probe (Jung and Schnitzer 2003). In this design, the optical magnification of the endoscope probe is close to unity for short working distances. *D*: an optical design in which the collimated laser beam pivots (signified by the curved dashed line) about the face of an endoscope probe with a relay lens of half-integral pitch. This angular deflection of the beam is converted into a lateral translation in the sample focal plane.

separated from the excitation beam by a dichroic mirror, and is captured by a photodetector (Figs. 6*A* and 7). Another variant uses a doublet probe with a ¾-pitch relay (Fig. 6*B*) for longer reach into deeper tissues. A third variant uses a GRIN micro-lens triplet probe (Fig. 6*C*) (Jung and Schnitzer 2003). The endoscope objective lens has a length less than ¼-pitch and a working distance ranging from 130–1,040 μm. The relay lens is an integral multiple of ½-pitch length and enables insertion into deep tissues. A third GRIN lens is an endoscope coupling lens of 0.5 *NA*, which matches the *NA* of a microscope objective lens that couples the laser beam into the endoscope probe (Fig. 6*C*). These design variants provide some flexibility in the optical and mechanical layout of a two-photon endoscope. Scanning is achieved by pivoting the collimated laser beam about the back aperture of the microscope objective (Fig. 6*C*) or achromatic lens (Fig. 6, *A* and *B*) that focuses the excitation beam onto the endoscope probe. This leads to lateral translation of the laser focal spot. An alternative strategy involves a collimated beam of narrow diameter that pivots about the external face of the endoscope probe (Fig. 6*D*). In this case, the endoscope consists of a GRIN objective lens and a ½-pitch GRIN relay, and the focal spot is again scanned laterally in the sample focal plane. Although initial (Jung and Schnitzer 2003) and subsequent (Levene et al. 2004) work involving compound GRIN micro-lenses for two-photon imaging has used triplet GRIN probes, after exploration of the various scanning strategies depicted in Fig. 6, we currently favor use of doublet GRIN lens probes (Fig. 6, *A* and *B*), which offer similar fields of view as the triplet probes but at about two-thirds the cost and with greater image magnification (4−6×) and lower *NA* for incoupling the laser beam. These optical advantages allow one to use a simple low *NA* achromat to couple the laser into a doublet endoscope probe, rather than a microscope objective of ~0.5 *NA*. Furthermore, the resulting weaker focus of the incoupled beam can help to reduce autofluorescence at the endoscope surface.

In vivo neuronal imaging using two-photon microendoscopy

Initial tests of in vivo two-photon microendoscopy involved anesthetized rats. We introduced Di-I into the ventral layers of CA1 and positioned the endoscope probe atop the hippocampal alveus. After sufficient time for the dye to diffuse dorsally, two-photon images revealed neuronal dendrites (Fig. 8*A*) in s. oriens. The sectioning capability of two-photon endoscopy was readily apparent during in vivo imaging, because micron-scale movements of the brain or of the endoscope probe brought individual dendritic features in s. oriens in and out of view with an axial sensitivity far surpassing that of one-photon microendoscopy. Further tests of imaging in CA1 involved anesthetized YFP-H mice expressing YFP in a subset of hippocampal pyramidal neurons (Feng et al. 2000). With an endoscope

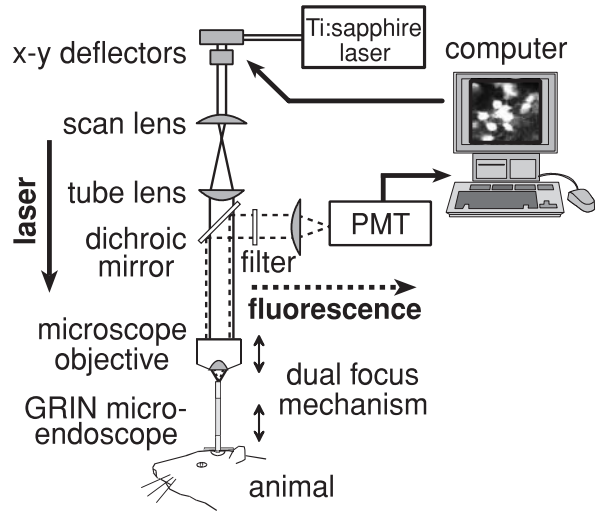

FIG. 7. Optical schematic of the two-photon endoscope. A Ti:sapphire laser emits ~100-fs pulses of infrared excitation light. The laser beam is steered in two angular dimensions by a pair of galvanometer-driven deflector mirrors and is expanded in a telescope comprised of a scan lens and a tube lens. Either a microscope objective or an achromat (not depicted) focuses the beam to a focal spot just above the external face of the endoscope probe. The probe refocuses the lateral scan pattern within the specimen. The focal plane in the specimen may be adjusted by moving either the endoscope probe itself or the microscope objective. This enables one to set the endoscope probe position and to acquire optical sections by adjusting only the position of the microscope objective. Fluorescence emissions (dashed lines) returning from the sample are separated from the excitation beam by a dichroic mirror and detected by a photomultiplier tube (PMT). A computer controls the galvanometer deflectors and reconstructs the image of the sample.

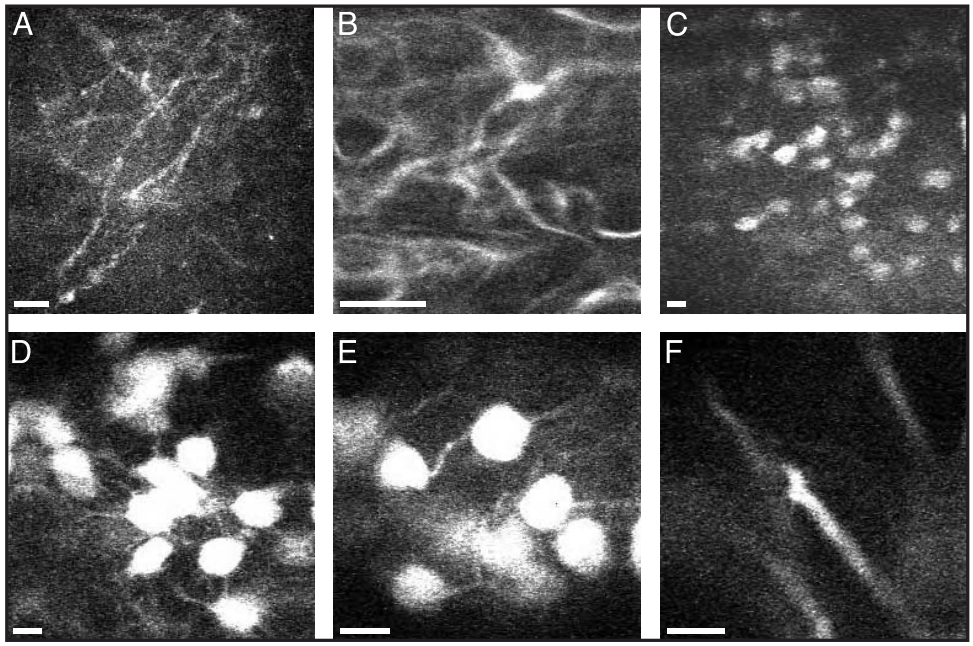

FIG. 8. Mammalian CA1 hippocampal neurons imaged in vivo with two-photon fluorescence microendoscopy. The endoscope probe is positioned atop the alveus in CA1. *A*: Di-I labeled dendrites in CA1 s. oriens of a live rat. The endoscope probe had a 1,000-μm diam, 0.48 *NA*, and a 130-μm *WD*. The image acquisition time was 0.77 s. *B–F*: in vivo two-photon microendoscopy images of fluorescent cell bodies, basal dendrites, and apical dendrites in CA1 s. pyramidale, s. oriens, and s. radiatum, respectively, in anesthetized YFP-H mice that express YFP in a subset of hippocampal pyramidal neurons (Feng et al. 2000). *B*: in vivo image of CA1 pyramidal cell basal dendrites in s. oriens. The endoscope probe had a 500-μm diam, 0.47 *NA*, and a 130-μm *WD*. Image acquisition time was 0.55 s. *C*: an image of over 25 pyramidal cell bodies taken with a 1,000-μm-diam endoscope with 1,040-μm *WD* and 0.38 *NA*. Image acquisition time was 0.38 s. *D*: in vivo image of pyramidal cell bodies using the same endoscope probe as in *C* but at higher digital magnification and with an acquisition time of 0.55 s. *E*: image of pyramidal cell bodies acquired in vivo with a 500-μm-diam endoscope probe, of 100-μm working distance and 0.47 *NA*. Image acquisition time was 0.55 s. *F*: two-photon image of larger dendrites in s. radiatum, ventral but proximal to s. pyramidale. The endoscope probe and acquisition time were identical to that used in *E*, but the digital magnification was increased. All scale bars are 10 μm.

probe positioned just dorsal to the hippocampal alveus, two-photon microendoscopy images of s. oriens revealed the basal dendrites of the fluorescent pyramidal cells (Fig. 8*B*).

Without repositioning the endoscope probe, images could be focused ventrally into CA1 s. pyramidale and beyond, into the dorsal portion of stratum radiatum up to about 270 μm below the alveus. Using digital zoom to set the spatial extent of the laser scan pattern, we could acquire individual endoscopic images of s. pyramidale that contained over ~25 pyramidal cell bodies at low magnification (Fig. 8*C*) or fewer cell bodies and greater dendritic details at higher magnifications (Fig. 8, *D* and *E*). At more ventral focal depths (~260 μm below alveus), we were able to visualize the larger apical dendritic trunks in s. radiatum (Fig. 8*F*). Without the optical sectioning capabilities of two-photon microendoscopy, it would otherwise be very difficult to isolate signals from an individual dendrite in s. radiatum without being overpowered by background fluorescence from the dense layer of fluorescent cell bodies dorsally overlying in s. pyramidale.

DISCUSSION

We constructed microendoscopes based on compound GRIN micro-lenses, which allowed us to perform high-resolution fluorescence imaging in mammalian brain areas that lie ~1 mm or more from the cranium, well beyond the imaging range of conventional in vivo microscopy. We employed these microendoscopes for in vivo fluorescence imaging of individual cells in hippocampus and in thalamus, deep brain areas that have been inaccessible to cellular imaging in live mammals. A major advantage of our imaging approach is that use of compound micro-lens probes allows us to place a mechanism for focal adjustment on the side of the probe that is external to the animal. In comparison, endoscopes based on individual or bundles of optical fiber must either operate at a fixed working distance (Dickensheets and Kino 1996; Knittel et al. 2001) or incorporate focusing mechanisms within the probe inserted into tissue (Rouse and Gmitro 2000; Sabharwal et al. 1999). Another key feature of our designs is the use of GRIN objective lenses with *NA* close to 0.5, providing lateral optical resolution as good as ~0.85 μm (Fig. 2), which we employed to discern subcellular details (Figs. 3, 4, 5, and 8). However, to date, we have been unable to visualize dendritic spines. Further improvements in resolution achieved by either raising the *NA* of the endoscope probes or by correcting for their optical aberrations will be necessary to resolve spines.

In this work, we have introduced one-photon fluorescence microendoscopy and its use in vivo. Our one-photon microendoscopy images (Figs. 3, 4, and 5) illustrate the potential offered by this technology for visualization of a wide variety of cell types with micron-scale resolution deep within tissues of live animals. One-photon microendoscopy is simpler to use and cheaper to construct than two-photon microendoscopy, and enables full-frame image capture for direct viewing of fluorescent cells through eyepieces or with a camera. Such full-frame detection opens the possibility of achieving fast-frame rate

imaging of cellular dynamics. The lack of optical sectioning inherent with this modality implies that signals from adjacent depths within tissue may be collected simultaneously, but the accompanying disadvantage is the presence of scattered and out of focus background fluorescence within the image.

We have exploited these properties of one-photon microendoscopy to produce video-rate movies of individual red blood cells flowing through hippocampal and thalamic capillaries in live rodents. Prior optical imaging studies of microcirculation were limited to vessels in the pia (Ma et al. 1974) and in the upper 250 μm (Villringer et al. 1994) to 600 μm (Kleinfeld et al. 1998) of mammalian neocortex. Using two-photon excitation, GRIN lenses, and one-dimensional laser line scans, blood cell speeds have been estimated deep within the neocortex (Levene et al. 2004), but this approach does not provide full frame movies or the individual trajectories of single blood cells. Microendoscopy studies of red blood cell dynamics in response to neural stimulation may help provide insight into mechanisms that couple nervous activity to hemodynamics and that underlie functional MRI (Ogawa et al. 1992), PET (Fox et al. 1986), and intrinsic signal imaging modalities (Malonek and Grinvald 1996).

Using one- and two-photon microendoscopy we have visualized deep brain neuronal cell bodies and dendrites in live rats and mice. The laser-scanning two-photon endoscope is particularly well suited for in vivo studies of subcellular structures such as individual neuronal dendrites (Fig. 8, *A* and *F*), because the instrument combines the ability of a two-photon microscope to sample thin optical sections with the ability of an endoscope to reach tissue areas millimeters deep below the surface. This combination should prove useful for in vivo imaging of fluorescent markers in a wide range of transgenic mouse lines. During both one- and two-photon microendoscopy (Figs. 5, *C* and *D*, and 8, *C–E*), multiple fluorescent cell bodies were visible within single image frames acquired in the CA1 area of transgenic YFP-H mice that express YFP within a subset of pyramidal neurons. As in our preliminary accounts (Jung et al. 2003), we report here two-photon imaging depths of $\sim$270 μm from the face of a GRIN microendoscope, sufficient to visualize individual dendrites in CA1 hippocampal s. radiatum in an adult mouse when a microendoscope probe is positioned just dorsal to the CA1 hippocampal alveus (Fig. 8*E*). The ability to image through such tissue depths has allowed us to visualize multiple anatomical layers without repositioning the microendoscope probe and compares favorably to a report of only $\sim$95 μm of imaging depth from the face of a GRIN lens probe (Levene et al. 2004). Nonetheless, our two-photon imaging depth of $\sim$270 μm is inferior to the $>$500 μm depths provided by conventional in vivo two-photon microscopy (Kleinfeld et al. 1998; Oheim et al. 2001). This difference almost certainly arises in large part due to the lower *NA* values of our microendoscope probes compared with those of commercially available water immersion microscope objective lenses, since the efficiency of fluorescence photon capture rises nonlinearly with *NA* (Yuste et al. 2000).

A small number of other studies in the live mammalian brain have used optical fibers or endoscopes. These studies either involved single optical fibers that did not provide images (Duff Davis and Schmidt 2000; Ikeda and Matsushita 1980; Kudo et al. 1992) or coarse-resolution endoscopes that were incapable of resolving individual cells and that relied on scattered light rather than fluorescence (Poe et al. 2003; Rector et al. 2001). In clinical practice, neuroendoscopes are used during aneurysm treatments (Wang et al. 2003) and intraventricular procedures (Anandh et al. 2001), but these endoscopes of 1–4 mm diam are designed for viewing millimeter-sized fields at low resolution. Miniature two-photon microscopes that can resolve individual cortical neurons currently remain too large to be used for microendoscopy (Helmchen et al. 2001).

The use of microendoscopes for imaging deep brain tissues in vivo differs from another recently introduced in vivo imaging methodology that relies on conventional microscope objectives and surgical removal of overlying brain tissue. Katz and colleagues have found that surgical removal of a portion of neocortical matter allows examination of the dorsal tissue of hippocampus by conventional two-photon microscopy (Mizrahi et al. 2004). After this surgical intervention, they have tracked the stability of hippocampal dendritic spines over several hours. Although such methodology employs water immersion objectives that offer superior resolution and higher *NA* than currently available GRIN micro-lenses provide, this invasive surgical approach may be limited in use to hippocampus or other structures within the working distance of the microscope objective from the cranium. For example, in vivo imaging of rat thalamus, which is about 4 mm ventral to the neocortical surface, would apparently require surgical removal of overlying neocortical and hippocampal tissue within a diameter broad enough to insert the microscope objective, thereby causing massive tissue disruption. An attempt to skirt this problem by use of a long working distance microscope objective and a small diameter tissue resection would limit the usable *NA* of the objective lens to that afforded by the geometry of the resection. Furthermore, surgical resection may preclude examination of certain issues that require study in a chronic preparation, because large-scale removal of afferents and efferents may induce long-term disturbance of neuronal properties. We have developed general methodologies for in vivo optical imaging of deep tissue such as thalamus (Fig. 3*C*) with high *NA* ($\sim$0.5) but without large-scale tissue resection.

Our methods rely on insertion of compound GRIN microlenses into tissue. Such microendoscopes of 350–1,000 μm diam are the smallest probes used to date for in vivo cellular imaging of which we are aware (Jung and Schnitzer 2003; Jung et al. 2003; Levene et al. 2004), but this diameter range exceeds that of microelectrodes. The micro-lenses are closer in size to microdialysis probes that are commonly used to study neurochemistry in vivo and that range from $\sim$250 μm and upward in diameter. Although the use of microendoscopes appears to be less invasive and more generally applicable than the surgical approaches developed by Mizrahi et al. 2004, future studies must consider the potential effects of the microendoscope probe on the biological phenomenon under consideration. Several potential strategies exist for inserting the endoscope probe in as minimally invasive a manner as possible, and two of these strategies have been explored to date.

The first strategy involves gradual insertion of the probe into the brain area of interest. We used this approach for studies of deep neocortical capillaries and neurons (Fig. 5*A*), and Levene et al. 2004 also adopted this tactic, employing stepwise increments sized a few tens of microns. However, insertion of a blunt optical probe will cause some degree of tissue distortion

and compression, which may create a spreading depression of neural activity (Bolay et al. 2002). Thus we also developed a second strategy that is intermediate between gradual probe insertion and gross resection and that seeks to minimize compression of the brain area under study. In this intermediate approach, a column of tissue overlying the brain area of interest is removed over a diameter comparable to that of the microendoscope probe. The microendoscope probe may be inserted through this opening without compressing the tissue to be visualized. The brain area under observation is left intact, and the probe is positioned just above. When this method was applied in the mouse brain, our imaging depth of up to $\sim$270 μm from the face of the endoscope probe allowed us to visualize cellular details in multiple hippocampal tissue layers (Fig. 8), without physically entering the hippocampus with the microendoscope probe. Furthermore, we have found that positioning the endoscope probe right above the structure of interest can have a stabilizing mechanical effect. We have often seen a discrete reduction in image distortion that accompanies an incremental mechanical advance of the probe, and we interpret this event as the endoscope probe just touching down on the brain tissue. In future in vivo imaging studies, the choice of whether to employ conventional microscopy and surgical resection, or microendoscopy with gradual probe insertion or minimal tissue removal, will largely depend on the particular brain area under study and the scientific requirements of the experiment. Further pursuit of all three approaches is needed to explore their relative strengths and weaknesses in detail. In microdialysis studies, a common tactic involves positioning the probe within a ventricle, and a similar approach might be fruitful for microendoscopy. Improvement of methods employing minimal tissue removal might involve use of a hypodermic guide tube, within which tissue is aspirated followed by insertion of the microendoscope through the tube.

The methods introduced here open possibilities for several distinct classes of in vivo experiments in deep brain tissues involving microendoscopy. One-photon microendoscopy should be particularly well suited for experiments that combine fast frame-rate imaging and the use of synthetic (Stosiek et al. 2003) or genetically encoded (Guerrero et al. 2002; Kuner and Augustine 2000; Truong et al. 2001) activity-dependent fluorescent probes, allowing neural activity to be monitored within multiple cell bodies simultaneously. Fluorescent gene reporters (Brown et al. 2001; Spergel et al. 2001) could be fruitfully visualized with either endoscopic modality, enabling studies of how environment, therapeutic agents, or specific patterns of brain activity affect gene expression. For determination of how such factors may alter fluorescent protein distributions within specific tissue laminae and cellular compartments, the sectioning capabilities and greater imaging depth offered by two-photon microendoscopy should make this modality the preferred choice. Our two-photon images of hippocampal pyramidal cells in the YFP-H mice revealed the presence of YFP within basal dendrites in s. oriens, cell bodies in s. pyramidale, and apical dendritic trunks in s. radiatum. Future in vivo imaging studies regarding laminar and cellular protein distributions would likely involve fluorescent protein fusions, such as those used to study somatodendritic patterns of cytoskeletal dynamics (Furuyashiki et al. 2002; Stepanova et al. 2003) and ion-channel localization (Antonucci et al. 2001) in vitro. Both microendoscopy modalities should also work well for combined optical and electrophysiological studies in which electrodes are targeted toward particular classes of neurons expressing fluorescent markers (Margrie et al. 2003). Finally, two-photon microendoscopy would generally be superior to its one-photon counterpart for tracking Ca^{2+} ion dynamics within individual dendrites using fluorescent Ca^{2+}-indicators, as performed previously using two-photon microscopy near the mammalian brain surface in combined imaging and electrophysiological studies (Charpak et al. 2001; Helmchen et al. 1999; Svoboda et al. 1997, 1999; Waters et al. 2003).

Further development of microendoscopy methodologies may enable chronic studies in which the long-term cellular effects of experience or of novel therapeutic treatments are repeatedly examined over prolonged time periods in tissues inaccessible to conventional microscopy. Fiber optic approaches (Helmchen et al. 2001) may extend our methods to freely moving animals. As new fluorescent probes of disease processes are created (Weissleder et al. 1999), potential clinical applications of microendoscopy should also emerge.

ACKNOWLEDGMENTS

We thank S. Block for providing an MBL/NNF test slide, G. Buzsaki for consultation on animal surgery, B. Messerschmidt for consultation on microlenses, K. Neumann for assistance affixing 170-nm beads to microscope slides, B. Flusberg for critical reading of the manuscript, and T. Nagaoka, W. Newsome, L. Stryer, and D. Tank for helpful conversations.

GRANTS

M. J. Schnitzer was supported by Bell Laboratories, Stanford University, a McKnight Technological Innovations in Neuroscience Award, the Human Frontier Science Program, and National Institute on Drug Abuse Grant 1R21DA-017895-01; J. C. Jung was supported in part by the Max Planck Institute for Medical Research; and A. D. Mehta is a Rett Syndrome Research Foundation Fellow of the Life Sciences Research Foundation.

DISCLOSURE

Lucent Technologies submitted patent applications based on the technology described here.

REFERENCES

Akaaboune M, Grady RM, Turney S, Sanes JR, and Lichtman JW. Neurotransmitter receptor dynamics studied in vivo by reversible photounbinding of fluorescent ligands. *Neuron* 34: 865–876, 2002.

Anandh B, Mohanty A, Sampath S, Praharaj SS, and Kolluri S. Endoscopic approach to intraventricular cysticercal lesions. *Minim Invasive Neurosurg* 44: 194–196, 2001.

Antonucci DE, Lim ST, Vassanelli S, and Trimmer JS. Dynamic localization and clustering of dendritic Kv2.1 voltage-dependent potassium channels in developing hippocampal neurons. *Neuroscience* 108: 69–81, 2001.

Balice-Gordon RJ and Lichtman JW. Long-term synapse loss induced by focal blockade of postsynaptic receptors. *Nature* 372: 519–524, 1994.

Beaurepaire E, Oheim M, and Mertz J. Ultra-deep two-photon fluorescence excitation in turbid media. *Opt Commun* 188: 25–29, 2001.

Bolay H, Reuter U, Dunn AK, Huang Z, Boas DA, and Moskowitz MA. Intrinsic brain activity triggers trigeminal meningeal afferents in a migraine model. *Nat Med* 8: 136–142, 2002.

Bozza T, McGann JP, Mombaerts P, and Wachowiak M. In vivo imaging of neuronal activity by targeted expression of a genetically encoded probe in the mouse. *Neuron* 42: 9–21, 2004.

Brown EB, Campbell RB, Tsuzuki Y, Xu L, Carmeliet P, Fukumura D, and Jain RK. In vivo measurement of gene expression, angiogenesis and physiological function in tumors using multiphoton laser scanning microscopy. *Nat Med* 7: 864–868, 2001.

Charpak S, Mertz J, Beaurepaire E, Moreaux L, and Delaney K. Odor-evoked calcium signals in dendrites of rat mitral cells. *Proc Natl Acad Sci USA* 98: 1230–1234, 2001.

Chen BE, Lendvai B, Nimchinsky EA, Burbach B, Fox K, and Svoboda K. Imaging high-resolution structure of GFP-expressing neurons in neocortex in vivo. *Learn Mem* 7: 433–441, 2000.

Chiu CS, Jensen K, Sokolova I, Wang D, Li M, Deshpande P, Davidson N, Mody I, Quick MW, Quake SR, and Lester HA. Number, density, and surface/cytoplasmic distribution of GABA transporters at presynaptic structures of knock-in mice carrying GABA transporter subtype 1-green fluorescent protein fusions. *J Neurosci* 22: 10251–10266, 2002.

Denk W and Svoboda K. Photon upmanship: why multiphoton imaging is more than a gimmick. *Neuron* 18: 351–357, 1997.

Diaspro A. *Confocal and Two-Photon Microscopy: Foundations, Applications, and Advances.* New York: Wiley-Liss, 2002.

Dickensheets DL and Kino GS. Micromachined scanning confocal optical microscope. *Opt Lett* 21: 764–766, 1996.

Dijkhuizen RM, Ren J, Mandeville JB, Wu O, Ozdag FM, Moskowitz MA, Rosen BR, and Finklestein SP. Functional magnetic resonance imaging of reorganization in rat brain after stroke. *Proc Natl Acad Sci USA* 98: 12766–12771, 2001.

Dirnagl U, Villringer A, and Einhaupl KM. In vivo confocal scanning laser microscopy of the cerebral microcirculation. *J Microscopy* 165: 147–157, 1992.

Duff Davis M and Schmidt JJ. In vivo spectrometric calcium flux recordings of intrinsic Caudate-Putamen cells and transplanted IMR-32 neuroblastoma cells using miniature fiber optrodes in anesthetized and awake rats and monkeys. *J Neurosci Meth* 99: 9–23, 2000.

Emkey WL and Jack CA. Analysis and evaluation of graded-index fiber-lenses. *J Lightwave Technol* 5: 1156–1164, 1987.

Feng G, Mellor RH, Bernstein M, Keller-Peck C, Nguyen QT, Wallace M, Nerbonne JM, Lichtman JW, and Sanes JR. Imaging neuronal subsets in transgenic mice expressing multiple spectral variants of GFP. *Neuron* 28: 41–51, 2000.

Fox PT, Mintun MA, Raichle ME, Miezin FM, Allman JM, and Van Essen DC. Mapping human visual cortex with positron emission tomography. *Nature* 323: 806–809, 1986.

Furuyashiki T, Arakawa Y, Takemoto-Kimura S, Bito H, and Narumiya S. Multiple spatiotemporal modes of actin reorganization by NMDA receptors and voltage-gated Ca^{2+} channels. *Proc Natl Acad Sci USA* 99: 14458–14463, 2002.

Gomez-Reino C, Perez MV, and Bao C. *Gradient-Index Optics.* Berlin: Springer-Verlag, 2002.

Grutzendler J, Kasthuri N, and Gan WB. Long-term dendritic spine stability in the adult cortex. *Nature* 420: 812–816, 2002.

Guerrero G, Siegel MS, Roska B, Loots E, and Isacoff EY. Tuning FlaSh: redesign of the dynamics, voltage range, and color of the genetically encoded optical sensor of membrane potential. *Biophys J* 83: 3607–3618, 2002.

Harris LW and Purves D. Rapid remodeling of sensory endings in the corneas of living mice. *J Neurosci* 9: 2210–2214, 1989.

Helmchen F, Fee MS, Tank DW, and Denk W. A miniature head-mounted two-photon microscope: high-resolution brain imaging in freely moving animals. *Neuron* 31: 903–912, 2001.

Helmchen F, Svoboda K, Denk W, and Tank DW. In vivo dendritic calcium dynamics in deep-layer cortical pyramidal neurons. *Nat Neurosci* 2: 989–996, 1999.

Hopt A and Neher E. Highly nonlinear photodamage in two-photon fluorescence microscopy. *Biophys J* 80: 2029–2036, 2001.

Hudetz AG, Biswal BB, Feher G, and Kampine JP. Effects of hypoxia and hypercapnia on capillary flow velocity in the rat cerebral cortex. *Microvasc Res* 54: 35–42, 1997.

Ikeda M and Matsushita A. Reflectance of rat-brain structures mapped by an optical fiber technique. *J Neurosci Meth* 2: 9–17, 1980.

Inoue S and Spring KR. *Video Microscopy: The Fundamentals.* New York: Plenum Press, 1986.

Ivanov KP, Kalinina MK, and Levkovich YuI. Microcirculation velocity changes under hypoxia in brain, muscles, liver, and their physiological significance. *Microvasc Res* 30: 10–18, 1985.

Jeromin A, Yuan LL, Frick A, Pfaffinger P, and Johnston D. A modified Sindbis vector for prolonged gene expression in neurons. *J Neurophysiol* 90: 2741–2745, 2003.

Jung JC, Aksay E, Hibino H, and Schnitzer MJ. In vivo epi-fluorescence micro-endoscopy. *Soc Neurosci Abstr* 404.20, 2002.

Jung JC, Mehta AD, and Schnitzer MJ. Multiphoton endoscopy: optical design and application to in vivo imaging of mammalian hippocampal neurons. Conference on Lasers and Electro-optics CThPDD5, 2003. Optical Society of America, Baltimore, MD.

Jung JC and Schnitzer MJ. In vivo epi-fluorescence micro-endoscopy. *Biophys J* 82: 496a, 2002.

Jung JC and Schnitzer MJ. Multiphoton endoscopy. *Opt Lett* 28: 902–904, 2003.

Kleinfeld D, Mitra PP, Helmchen F, and Denk W. Fluctuations and stimulus-induced changes in blood flow observed in individual capillaries in layers 2 through 4 of rat neocortex. *Proc Natl Acad Sci USA* 95: 15741–15746, 1998.

Knittel J, Schnieder L, Buess G, Messerschmidt B, and Possner T. Endoscope-compatible confocal microscope using a gradient index-lens system. *Opt Commun* 188: 267–273, 2001.

Kogelnik H. Imaging of optical modes—resonators with internal lenses. *AT&T Tech J* 44: 455–494, 1965.

Kudo Y, Akita K, Nakamura T, Ogura A, Makino T, Tamagawa A, Ozaki K, and Miyakawa A. A single optical fiber fluorometric device for measurement of intracellular Ca^{2+} concentration: its application to hippocampal neurons in vitro and in vivo. *Neuroscience* 50: 619–625, 1992.

Kuner T and Augustine GJ. A genetically encoded ratiometric indicator for chloride: capturing chloride transients in cultured hippocampal neurons. *Neuron* 27: 447–459, 2000.

Levene MJ, Dombeck DA, Kasischke KA, Molloy RP, and Webb WW. Multi-photon imaging of deep tissue using gradient index lenses. *Soc Neurosci Abstr* 403.15, 2002.

Levene MJ, Dombeck DA, Kasischke KA, Molloy RP, and Webb WW. In vivo multiphoton microscopy of deep brain tissue. *J Neurophysiol* 91: 1908–1912, 2004.

Levene MJ, Dombeck DA, Molloy RP, Kasischke KA, and Webb WW. Multi-photon microscopy of deep tissue with gradient index lenses. Conference on Lasers and Electro-optics: CTu02, 2003. Optical Society of America, Baltimore, MD.

Lippincott-Schwartz J and Patterson GH. Development and use of fluorescent protein markers in living cells. *Science* 300: 87–91, 2003.

Ma YP, Koo A, Kwan HC, and Cheng KK. Online measurement of the dynamic velocity of erythrocytes in cerebral microvessels in the rat. *Microvasc Res* 8: 1–13, 1974.

Mack V, Burnashev N, Kaiser KM, Rozov A, Jensen V, Hvalby O, Seeburg PH, Sakmann B, and Sprengel R. Conditional restoration of hippocampal synaptic potentiation in Glur-A-deficient mice. *Science* 292: 2501–2504, 2001.

Malonek D and Grinvald A. Interactions between electrical activity and cortical microcirculation revealed by imaging spectroscopy: implications for functional brain mapping. *Science* 272: 551–554, 1996.

Margrie TW, Meyer AH, Caputi A, Monyer H, Hasan MT, Schaefer AT, Denk W, and Brecht M. Targeted whole-cell recordings in the mammalian brain in vivo. *Neuron* 39: 911–918, 2003.

Martin C, Berwick J, Johnston D, Zheng Y, Martindale J, Port M, Redgrave P, and Mayhew J. Optical imaging spectroscopy in the unanaesthetised rat. *J Neurosci Meth* 120: 25–34, 2002.

Messerschmidt B, Possner U, and Houde-Walter SN. Fabrication tolerances and metrology requirements for ion-exchanged micro-optic lenses: what's good enough? *Appl Optics* 36: 8145–8152, 1997.

Miyawaki A, Sawano A, and Kogure T. Lighting up cells: labelling proteins with fluorophores. *Nat Cell Biol Suppl* 5: S1–S7, 2003.

Mizrahi A, Crowley JC, Shtoyerman E, and Katz LC. High-resolution in vivo imaging of hippocampal dendrites and spines. *J Neurosci* 24: 3147–3151, 2004.

Ng M, Roorda RD, Lima SQ, Zemelman BV, Morcillo P, and Miesenbock G. Transmission of olfactory information between three populations of neurons in the antennal lobe of the fly. *Neuron* 36: 463–474, 2002.

Ogawa S, Tank DW, Menon R, Ellermann JM, Kim SG, Merkle H, and Ugurbil K. Intrinsic signal changes accompanying sensory stimulation: functional brain mapping with magnetic resonance imaging. *Proc Natl Acad Sci USA* 89: 5951–5955, 1992.

Oheim M, Beaurepaire E, Chaigneau E, Mertz J, and Charpak S. Two-photon microscopy in brain tissue: parameters influencing the imaging depth. *J Neurosci Meth* 111: 29–37, 2001.

Okubo Y, Kakizawa S, Hirose K, and Iino M. Visualization of IP(3) dynamics reveals a novel AMPA receptor-triggered IP(3) production pathway mediated by voltage-dependent Ca(2+) influx in Purkinje cells. *Neuron* 32: 113–122, 2001.

Oldenbourg R, Inoue S, Tiberio R, Stemmer A, Mei G, and Skvarla M. Standard test targets for high-resolution light microscopy. In: *Nanofabrica-*

tion and Biosystems: Integrating Materials Science, Engineering and Biology, edited by Hoch HC, Jelinsky LW, and Craighead HG. Cambridge, UK: Cambridge Univ Press, p. 123–138, 1996.

Oldenbourg R, Terada H, Tiberio R, and Inoue S. Image sharpness and contrast transfer in coherent confocal microscopy. *J Microscopy* 172: 31–39, 1993.

Oliva AA Jr, Jiang M, Lam T, Smith KL, and Swann JW. Novel hippocampal interneuronal subtypes identified using transgenic mice that express green fluorescent protein in GABAergic interneurons. *J Neurosci* 20: 3354–3368, 2000.

Poe GR, Rector DM, and Harper RM. State-dependent columnar organization of dorsal hippocampal activity in the freely-behaving cat. *Behav Brain Res* 138: 107–112, 2003.

Pomeroy SL and Purves D. Neuron/glia relationships observed over intervals of several months in living mice. *J Cell Biol* 107: 1167–1175, 1988.

Purves D and Lichtman JW. Synaptic sites on reinnervated nerve cells visualized at two different times in living mice. *J Neurosci* 7: 1492–1497, 1987.

Purves D, Voyvodic JT, Magrassi L, and Yawo H. Nerve terminal remodeling visualized in living mice by repeated examination of the same neuron. *Science* 238: 1122–1126, 1987.

Rector DM, Rogers RF, Schwaber JS, Harper RM, and George JS. Scattered-light imaging in vivo tracks fast and slow processes of neurophysiological activation. *Neuroimage* 14: 977–994, 2001.

Reed WA, Yan MF, and Schnitzer MJ. Gradient-index fiber-optic microprobes for minimally invasive in vivo low-coherence interferometry. *Opt Lett* 27: 1794–1796, 2002.

Rouse AR and Gmitro AF. Multispectral imaging with a confocal microendoscope. *Opt Lett* 25: 1708–1710, 2000.

Sabharwal YS, Rouse AR, Donaldson L, Hopkins MF, and Gmitro AF. Slit-scanning confocal microendoscope for high-resolution in vivo imaging. *Appl Optics* 38: 7133–7144, 1999.

Sato M, Ozawa T, Inukai K, Asano T, and Umezawa Y. Fluorescent indicators for imaging protein phosphorylation in single living cells. *Nat Biotechnol* 20: 287–294, 2002.

Shtoyerman E, Arieli A, Slovin H, Vanzetta I, and Grinvald A. Long-term optical imaging and spectroscopy reveal mechanisms underlying the intrinsic signal and stability of cortical maps in V1 of behaving monkeys. *J Neurosci* 20: 8111–8121, 2000.

Spergel DJ, Kruth U, Shimshek DR, Sprengel R, and Seeburg PH. Using reporter genes to label selected neuronal populations in transgenic mice for gene promoter, anatomical, and physiological studies. *Prog Neurobiol* 63: 673–686, 2001.

Stepanova T, Slemmer J, Hoogenraad CC, Lansbergen G, Dortland B, De Zeeuw CI, Grosveld F, van Cappellen G, Akhmanova A, and Galjart N. Visualization of microtubule growth in cultured neurons via the use of EB3-GFP (end-binding protein 3-green fluorescent protein). *J Neurosci* 23: 2655–2664, 2003.

Stosiek C, Garaschuk O, Holthoff K, and Konnerth A. In vivo two-photon calcium imaging of neuronal networks. *Proc Natl Acad Sci USA* 100: 7319–7324, 2003.

Svoboda K, Denk W, Kleinfeld D, and Tank DW. In vivo dendritic calcium dynamics in neocortical pyramidal neurons. *Nature* 385: 161–165, 1997.

Svoboda K, Helmchen F, Denk W, and Tank DW. Spread of dendritic excitation in layer 2/3 pyramidal neurons in rat barrel cortex in vivo. *Nat Neurosci* 2: 65–73, 1999.

Theer P, Hasan MT, and Denk W. Two-photon imaging to a depth of 1000 microns in living brains by use of a Ti:Al2O3 regenerative amplifier. *Opt Lett* 28: 1022–1024, 2003.

Trachtenberg JT, Chen BE, Knott GW, Feng G, Sanes JR, Welker E, and Svoboda K. Long-term in vivo imaging of experience-dependent synaptic plasticity in adult cortex. *Nature* 420: 788–794, 2002.

Truong K, Sawano A, Mizuno H, Hama H, Tong KI, Mal TK, Miyawaki A, and Ikura M. FRET-based in vivo Ca^{2+} imaging by a new calmodulin-GFP fusion molecule. *Nat Struct Biol* 8: 1069–1073, 2001.

Villringer A, Them A, Lindauer U, Einhaupl K, and Dirnagl U. Capillary perfusion of the rat brain cortex. An in vivo confocal microscopy study. *Circ Res* 75: 55–62, 1994.

Walsh MK and Lichtman JW. In vivo time-lapse imaging of synaptic takeover associated with naturally occurring synapse elimination. *Neuron* 37: 67–73, 2003.

Wang E, Yong NP, and Ng I. Endoscopic assisted microneurosurgery for cerebral aneurysms. *J Clin Neurosci* 10: 174–176, 2003.

Waters J, Larkum M, Sakmann B, and Helmchen F. Supralinear Ca^{2+} influx into dendritic tufts of layer 2/3 neocortical pyramidal neurons in vitro and in vivo. *J Neurosci* 23: 8558–8567, 2003.

Weissleder R, Tung CH, Mahmood U, and Bogdanov A Jr. In vivo imaging of tumors with protease-activated near-infrared fluorescent probes. *Nat Biotechnol* 17: 375–378, 1999.

Yuste R, Lanni F, and Konnerth A. *Imaging Neurons: A Laboratory Manual*. Cold Spring Harbor, NY: Cold Spring Harbor Laboratory Press, 2000.

Zhang J, Campbell RE, Ting AY, and Tsien RY. Creating new fluorescent probes for cell biology. *Nat Rev Mol Cell Biol* 3: 906–918, 2002.